MedChemComm

RESEARCH ARTICLE

View Article Online
View Journal

Cite this: DOI: 10.1039/c6md00293e

Deferasirox-coated iron oxide nanoparticles as a potential cytotoxic agent†

Faezeh Taghavi,[a] Amir Sh. Saljooghi,*[a] Mostafa Gholizadeh[a] and Mohammad Ramezani[b]

Two broad strategies for the use of iron chelators in cancer treatment have been explored. The first was using iron chelators to reduce the iron level in cancer cells. Cancer cells typically require more iron than normal cells to mediate their generally rapid DNA synthesis and growth. The second more recent strategy is using chelators that help the redox cycling of iron to generate cytotoxic ROS (reactive oxygen species) within tumors. Both methods are currently being pursued. Deferasirox is an FDA-approved medication used to reduce chronic iron overload. Because of the low toxicity and oral administration of deferasirox, the use of this drug in cancer therapy is a new approach. Therefore, a number of recent studies have examined the potential of deferasirox as an anticancer agent. According to these strategies, the present study has reported the new role of deferasirox (DFX) loaded on iron oxide nanoparticles (Fe_3O_4@DFX) as an anticancer agent. The cytotoxicity of Fe_3O_4@DFX was screened against MCF-7, HeLa, HT-29, K-562, Neuro-2a, and L-929 cell lines by MTT assay. The surface of magnetic nanoparticles (MNPs) was first coated with (3-aminopropyl) trimethoxysilane (APTMS) and was then linked with deferasirox *via* an amidation reaction between $-NH_2$ and –COOH to form well-dispersed surface-functionalized biocompatible MNPs. The obtained nanoparticles were thoroughly characterized by various spectroscopic and microscopic methods such as SEM, FT-IR, TGA and VSM. Because of the ability of magnetic nanoparticles in biomedical applications to be targeted toward the site of action using magnetic field gradients, we suggest that MNPs loaded with deferasirox could be considered as a potential formulation, which can simultaneously be used as a theranostic agent for both cancer treatment and imaging. The obtained results provide experimental evidence that magnetite nanoparticles loaded with deferasirox induce apoptosis in cancer cell lines. Moreover, flow cytometry results confirm that the investigated compound produces a high population of apoptotic cells (69.3%), 1.2 fold higher than cisplatin (58.1%) at the same concentration, and could induce apoptosis in human leukemia cell lines (K-562).

Received 29th May 2016,
Accepted 18th August 2016

DOI: 10.1039/c6md00293e

www.rsc.org/medchemcomm

1. Introduction

Recent research and development has focused on the increasingly growing area of nanotechnology in modern science. Nanomaterials, with special chemical and physical properties, have many advantages.[1] Magnetic nanomaterials, with their unusual characteristics, are applied to cell separation,[2] immunoassay, magnetic resonance imaging (MRI),[3] drug and gene delivery,[4] minimally invasive surgery,[5] hyperthermia, and artificial muscle applications.[6] Also, nanoparticles have a main role in drug delivery to target tissues and to enhance stability against degradation by enzymes.[7] The superparamagnetic nanoparticle, as one of these nanoparticles, can be manipulated by an external magnetic field, which directs it to the target tissue.[8] Superparamagnetic nanoparticles, due to their unique mesoscopic physical, chemical, thermal, and mechanical properties, offer a high potential for several biomedical applications,[9] including: (a) cellular therapy, such as cell labelling and targeting, and as a suitable tool to perform cell biology studies involving the isolation and purification of cell populations;[10] (b) tissue repair; (c) magnetic field-guided carriers for localizing drugs or radioactive therapies;[11] (e) tumor hyperthermia.[12] Drugs, proteins, enzymes, antibodies, and nucleotides are directed to an organ, tissue, or tumor by linking them to magnetic nanoparticles.[13,14] The diffusion coefficient and the biodegradation rate are two main factors in the release mechanism of drugs that govern the drug release

[a] *Department of Chemistry, Ferdowsi University of Mashhad, P. O. Box 91775-1436, Mashhad, Iran. E-mail: saljooghi@um.ac.ir; Tel: +98 513880 5527*
[b] *Pharmaceutical Research Center, School of Pharmacy, Mashhad University of Medical Sciences, Mashhad, Iran*
† The authors declare no competing interests.

rate. The binding of drugs to the nanoparticles was investigated, either in the preparation stage of nanoparticles or by adsorption of drugs on the nanoparticles.[7]

The compound, (3-aminopropyl) trimethoxysilane (APTMS), is widely used to promote the interfacial behaviour of inorganic oxides, including silica,[15,16] ceramics,[17] titania,[18] and magnetic iron oxide nanoparticles (MNP_s).[19] Also, APTMS has been especially attractive for biological applications, such as drug delivery, and is widely used because of its amino functional group.[20–23]

This work describes APTMS-modified MNPs as a novel support for 4-[3,5-bis(2-hydroxyphenyl)-1,2,4-triazol-1-yl]-benzoic acid (deferasirox) loading for anticancer studies. The deferasirox was covalently bound to APTMS assembled on the MNPs surface through an amidation reaction between the carboxylic acid end groups on deferasirox and the pendant amine group on the capping linker. Based on previous investigations, the drug cleaved from the nanoparticles inside cells.[24]

The synthesis of deferasirox, (DFX or ICL670) was first reported in 1999.[25] In 2005, deferasirox became the first FDA-approved oral alternative for the treatment of iron overload and was subsequently approved in the EU in 2006.[26] This iron chelator is used for the treatment of iron overload in certain types of anemia, such as that caused by β-thalassemia, and the treatment of other toxic metal overload.[27,28] Cancer cells typically require more iron than normal cells to mediate their generally rapid DNA synthesis and growth.[29] The main aim of the present study was to investigate the potential antitumor activity of deferasirox loaded on iron oxide nanoparticles *via* APTMS as a spacer with no chelated iron ions.

2. Experimental

2.1. Chemicals

All solvents were purchased from Merck Co. Triethylamine (NEt_3), 4-hydrazino-benzoic acid, and 2-(2-hydroxyphenyl)-4*H*-3,1-benzoxazin-4-one were purchased from Merck without further purification; 1-ethyl-3-[3-dimethylaminopropyl]carbodiimide hydrochloride (EDC) and 7-hydroxybenzotriazole hydrate (HOBt) were purchased from Fluka (Germany).

RPMI-1640 medium, Dulbecco's modified eagle's medium (DMEM) and fetal bovine serum (FBS) were purchased from GIBCO (Gaithersburg, USA). Penicillin and streptomycin were purchased from Biochrom AG (Berlin, Germany). MTT (3-(4,5-dimethylthiazol-2-yl)-2,5-diphenyltetrazolium bromide, a yellow tetrazole) was purchased from Sigma Co., Ltd. Cisplatin was purchased from Sigma Aldrich.

2.2. Apparatus

NMR spectra were recorded on Avance Bruker-400 MHz spectrometers. All chemical shifts in NMR experiments are reported as ppm and were referenced to residual solvent. Chemical shifts are reported in parts per million and the signals are quoted as s (singlet), br (broad), d (doublet) and m (multiplet). FT-IR spectra were recorded on an AVATAR-370-FTIR Thermo Nicolet instrument. All mass spectra were scanned on a Varian Mat CH-7 instrument at 70 eV. Reactions were monitored by TLC using silica gel plates and the products were identified by comparison of their spectra and physical data with those of authentic samples. Melting points were measured on an Electrothermal 9100 apparatus. Scanning electron microscopy (SEM) images were taken on a Zeiss LEO 1450 VP/35Kv instrument, Germany. Thermogravimetric analysis (TGA) was carried out using thermogravimetric analyzer TGA-50 (Shimadzu Japan) instruments. Elemental analysis was carried out using a CHNS (O) Analyzer Model FLASH EA 1112 series made by Thermo Finnigan, Italy. Magnetization values were obtained by using a vibrating sample magnetometer (VSM), 7400 Lake Shore, America.

2.3. Synthesis of 4-[3,5-bis(2-hydroxyphenyl)-1,2,4-triazol-1-yl] benzoic acid (deferasirox)

The compound, 2-(2-hydroxyphenyl)-4*H*-3,1-benzoxazin-4-one was prepared according to a previously reported procedure with some modifications.[30,31] The compounds, 4-hydrazinobenzoic acid (11.5 mmol, 1.75 g) and Et_3N (11.5 mmol, 1.16 g) were dissolved in boiling EtOH (80 mL). Then, 2-(2-hydroxyphenyl)-4*H*-3,1-benzoxazin-4-one (10.45 mmol, 2.50 g) was added to the clear solution, and the reaction mixture was refluxed for an additional 2 h. After completion of the reaction, the solution was cooled down to room temperature, and water was added until the first sign of precipitation was observed. The mixture was then concentrated to a total volume of 50% under reduced pressure, and aqueous 6 M HCl (40 mL) was added. The resulting solid was filtered, washed with water and dried for 24 h in vacuum. Yellow powder; (3.11 g, yield = 80%); m.p. 264–266 °C; IR (KBr) *ν*: 3317, 2540, 1680 (C═O), 1607, 1517, 1495, 1431, 1351, 1221, 988, 752 cm^{-1}; ^1H NMR (C_3H_6O-$d_6$400 MHz): δ 7.00 (s, 1H), 7.01–7.04 (m, 3H), 7.39 (m, 2H), 7.48 (d, 1H), 7.53 (d, 2H), 8.15 (d, 2H), 8.19 (d, 1H) 10.00 (s, OH), 10.78 (s, OH) ppm; ^{13}C NMR (C_3H_6O-d_6, 75 MHz): δ 113.7, 113.9, 116.6 (CH), 117.0 (CH), 119.5 (CH), 119.8 (CH), 124.0 (2 CH), 126.9 (CH), 130.4 (2 CH), 130.5, 130.7 (CH), 131.4 (CH), 132.6, 141.9 (CH), 152.1, 155.6, 156.4, 160.4, 165.7 (C═O) ppm; M.S. (70 eV) *m*/*z* (%): 374 (M+); anal. calc. for $C_{21}H_{15}N_3O_4$: C, 67.56; H, 4.05; N, 11.25. Found: C, 67, 76; H, 3.85; N, 11.14.

2.4. Synthesis of Fe_3O_4 NP_S

The magnetite nanoparticles (Fe_3O_4 MNPs) were synthesized by a reported chemical co-precipitation technique with ferric and ferrous ions in alkaline solution, with some modifications.[32,33] $FeCl_2{\cdot}4H_2O$ (9.25 mmol) and $FeCl_3{\cdot}6H_2O$ (15.8 mmol) were dissolved in deionized water (150 mL) under Ar atmosphere at room temperature. An NH_4OH solution (25%, 50 mL) was then added dropwise (drop rate = 1 mL min^{-1}) to the stirring mixture at room temperature to reach a reaction pH of 11. The resulting black dispersion was continuously

stirred for 1 h at room temperature and then collected by magnet.

2.5. Surface coating of MNPs by APTMS (MNP-APTMS)

The silanization of magnetic nanoparticles with APTMS (MNP-APTMS) was done according to a previously reported procedure by Lui *et al.*[34]

The MNPs were dispersed in 100 mL of methanol/toluene (volume ratio, 1 : 1) as solvent and then sonicated for 30 min and heated up to 95 °C until 50 mL of the solvent was evaporated. Thereafter, methanol (50 mL) was added. The operation was repeated three times to ensure that the solution was completely anhydrous. Subsequently, the volume of reaction mixture was fixed at 100 mL by the addition of methanol followed by APTMS addition and stirred for a certain time (30 min) at 30 or 70 °C under N_2. The product was washed several times with anhydrous ethanol and distilled water by magnetic decantation and dried under vacuum. The product was washed with toluene and Soxhlet extraction was performed for 24 h and finally, it was dried at 40–50 °C for 6 h.

2.6. The reaction of APTMS surface-functionalized MNPs with deferasirox

Deferasirox (4.2 mmol) was dissolved in 100 ml of toluene and was then added to 1.1 g of the previous sample in the presence of EDC (50 mg)/HOBt (40 mg) to activate the carboxylate groups of deferasirox for amide bond formation.[35] EDC/HOBt (also NHS) crosslinking leads to amide bond formation between activated carboxyl groups and amine groups. This mixture was refluxed under stirring for 24 h and was then filtered and washed with 100 ml of dry toluene (Soxhlet extraction) for 24 h. The solid product was dried at room temperature under vacuum and is abbreviated as MNP-APTMS-DFX. The preparation procedure for deferasirox-loaded iron oxide nanoparticles is shown in Scheme 1.

3. Biological studies

3.1. Cell culture methods

Human breast cancer cells MCF-7 (ATCC HTB-22), human cervical epithelial carcinoma HeLa (ATCC CCL-2), human colon cancer cell line HT-29 (ATCC HTB-38), human leukemia cell line K-562 (ATCC CCL-243), mouse neuroblastoma cell line Neuro-2a (ATCC CCL-131), and mouse fibroblast L-929 cell line (ATCC CCL-1) were obtained from the American Type Culture Collection (ATCC; Manassas, VA, USA) and cultured at 37 °C in a humidified atmosphere of 5% CO_2 in air. HeLa cells were cultured in Dulbecco's modified eagle's medium (DMEM) with 0.1 mM nonessential amino acids, 2 mM glutamine, 1.0 mM sodium pyruvate, and 5% fetal bovine serum, at 37 °C in an atmosphere of 5% CO_2. Cells were plated in 96-well sterile plates at a density of 1×10^4 cells per well in 100 μL of medium and incubated for 1 h. Also, MCF-7 and HT-29 cells were cultured in Dulbecco's modified eagle's medium (DMEM) containing 10% fetal bovine serum, 100 units per mL of penicillin and 100 μg mL^{-1} of streptomycin. L-929 and K-562 cells were cultured in RPMI-1640 containing 10% fetal bovine serum, 100 units per mL of penicillin and 100 μg mL^{-1} of streptomycin. This study was approved by the Ethics Committee of Ferdowsi University of Mashhad, Mashhad, Iran and the Pharmaceutical Research Center, School of Pharmacy, Mashhad University of Medical Sciences, Mashhad, Iran. Also, basic pre-clinical research is needed before these can be recommended for human administration.

3.2. MTT assay in human cancer cell lines

Fe_3O_4-APTMS-DFX was tested for cytotoxic activity against human breast cancer cells (MCF-7), human cervical epithelial carcinoma (HeLa), human colon cancer cell line (HT-29), human leukemia cell line (K-562), and mouse neuroblastoma cell line (Neuro-2a); mouse fibroblast, L-929 cell line, and cisplatin was used as a comparative standard by MTT assay. Cell viability was evaluated by using a colorimetric method based

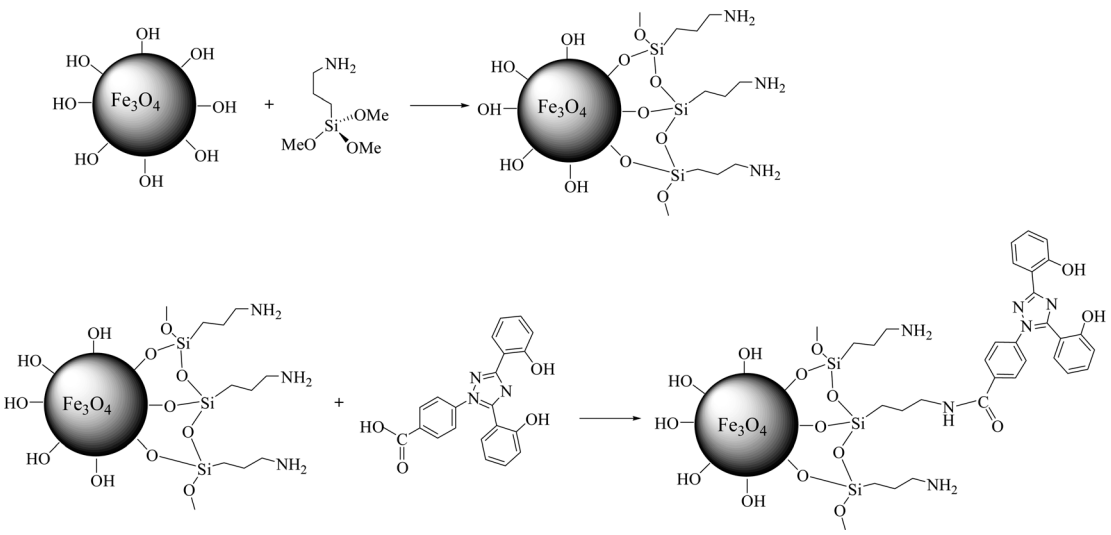

Scheme 1 Preparation procedure of deferasirox-loaded iron oxide nanoparticles.

on the tetrazolium salt, MTT [3-(4,5-dimethylthiazol-2-yl)-2,5-diphenyl tetrazolium bromide], which is reduced by living cells to yield purple formazan crystals. Cells were seeded in 96-well plates at a density of 2–5 × 10^4 cells of MCF-7, HeLa, HT-29, K-562, Neuro-2a and L-929 per well in 200 μL of culture medium and left to incubate overnight for optimal adherence. After careful removal of the medium, 200 μL of a dilution series of Fe_3O_4-APTMS-DFX in fresh medium were added and incubation was performed at 37 °C/5% CO_2 for 72 h. Fe_3O_4-APTMS-DFX was first solubilized in DMSO, diluted in medium and added to the cells in final concentrations between 20 nM and 200 μM. The percentage of DMSO in the cell culture medium did not exceed 0.3%.[36] Cisplatin was first solubilized in saline and was then added at the same concentrations used for the other compounds. At the end of the incubation period, the conjugate was removed and the cells were incubated with 200 μL of MTT solution (500 μg ml^{-1}). After 3–4 h at 37 °C, 5% CO_2, the medium was removed and the purple formazan crystals were dissolved in 200 μL of DMSO by shaking. The cell viability was evaluated by measurement of the absorbance at 570 nm using a STAT FAX-2100 microplate reader (Awareness Technology, Palm City, FL, USA). The cell viability was calculated by dividing the absorbance of each well by that of the control wells (cells treated with medium containing 0.3% DMSO). Each experiment was repeated at least three times and each point was determined from at least three replicates.

3.3. Apoptosis assay for compound MNP-APTMS-DFX by flow cytometry

Evaluation of apoptosis by flow cytometry is generally accomplished by methods that use annexin V-FITC as vital dye, which binds phosphatidyl serine exposed on the cell surface at the beginning of this process. The differentiation between apoptotic and necrotic cells can be performed by simultaneous staining with propidium iodide (PI). Therefore, annexin V-FITC was used as a marker of phosphatidyl serine and PI as a marker for dead cells. This combination allows differentiation among early apoptotic cells (annexin V-positive, PI-negative), late apoptotic/necrotic cells (annexin V-positive, PI-positive), and viable cells (annexin V-negative, PI-negative).

Cells lines (5 × 10^5) were seeded, treated with the conjugate (Fe_3O_4-APTMS-DFX) and incubated for 24 h at a concentration close to the IC_{50} at 37 °C. Following treatment, the cells were harvested by trypsinization and centrifugation at 1000 rpm for 5 min. The supernatant was removed, and the cell pellet was washed in PBS, followed by two washes in binding buffer (10 mM HEPES, 150 mM NaCl, 5 mM KCl, 1.8 mM $CaCl_2$, 1 mM $MgCl_2$). The cells were incubated with an annexin V/FITC antibody (5 ml in 100 ml binding buffer) at 4 °C for 15 min in the dark. Samples were washed in binding buffer, and the supernatant was discarded. The pellet was resuspended in 490 ml binding buffer, and 10 ml propidium iodide (10 mg ml^{-1} in PBS) was added to the samples before analysis by flow cytometry. Flow cytometry was performed with a Partec PAS flow cytometer (Partec GmbH, Germany) with Fe_3O_4-APTMS-DFX and cisplatin as a reference.

Also, apoptosis was detected using an *in situ* cell death detection kit (Boehringer Mannheim Corp., Indianapolis, IN), as described by Narla *et al.* and Zhu *et al.* Cells were incubated with all compounds in 0.3% DMSO or 1 : 16 diluted plasma samples from DFX-treated mice for 48 h at 37 °C, and were fixed, permeabilized, incubated with a reaction mixture containing TdT- and FITC-conjugated dUTP, and counterstained with propidium iodide. Cells were transferred to slides and viewed with a confocal laser scanning microscope (Bio-Rad MRC 1024) mounted on a Nikon Eclipse E800 series upright microscope, as reported previously.[37,38]

3.4. Statistical analysis

IC_{50} values were expressed as mean ± standard deviation (SD) from at least three independent experiments. Statistical tests, including one-way ANOVA, Tukey multiple comparison, or unpaired Student's *t*-tests were performed using SPSS, version 17 software. A *p* value of less than 0.05 was considered significant.

4. Results

The present study has reported the synthesis of iron oxide-based deferasirox (DFX) loaded nanoparticles (Fe_3O_4@DFX). The surface of the magnetic nanoparticles (MNPS) was first coated with (3-aminopropyl)trimethoxysilane (APTMS) and was then linked with deferasirox *via* the amidation reaction between $–NH_2$ and –COOH to form well-dispersed surface-functionalized biocompatible MNPs. The obtained nanoparticles were thoroughly characterized by various spectroscopic and microscopic methods, such as SEM, FT-IR, TGA, and VSM.

4.1. Characterization of deferasirox-loaded magnetic nanoparticles (MNP-APTMS-DFX)

The conjugates were thoroughly characterized using various spectroscopic and microscopic methods, such as FT-IR, TGA, and SEM-EDS.

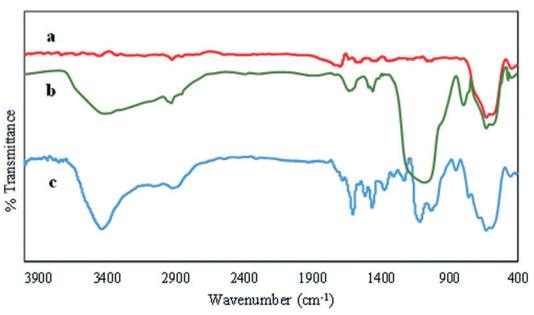

Fig. 1 (a) Infrared spectra of magnetic nanoparticles (MNPs), (b) MNPs modified with 3-(aminopropyl)trimethoxysilane (MNP-APTMS) and (c) deferasirox anchored on MNP-APTMS (MNP-APTMS-DFX).

Fig. 1 shows the FT-IR spectrum of as-synthesized MNP-APTMS-DFX. Uncoated Fe_3O_4 MNPs Fig. 1(a) show a broad peak around 580 cm^{-1} due to the stretching of Fe–O bonds.[39] Fig. 1(b) shows the FT-IR spectrum of Fe_3O_4-APTMS; the characteristic peaks of Fe_3O_4 are shifted to 597 cm^{-1}. The bands at 1030 and 935 cm^{-1} could be attributed to the stretching vibration of the Si–O bond. C–N stretching vibration and N–H bending bands appeared at 1150 and 1550 cm^{-1}.[40] The peaks around 2910 cm^{-1} and a broad absorption peak around 3430 cm^{-1} could be attributed to the stretching vibrations of CH_2 and NH_2 groups, respectively. The FT-IR spectrum of Fe_3O_4-APTMS-DFX (Fig. 1(c)) indicates new peaks at 1462, 1605, and 1683 cm^{-1} due to the aromatic C=C stretch and C=N stretch of deferasirox. Furthermore, an amide carbonyl group appears at 1710 cm^{-1}. C–H stretching of aromatic systems and propyl groups is observed at 2921–3100 cm^{-1}. The broad absorption peak at 3435 cm^{-1} is attributed to the O–H groups of deferasirox and the N–H stretching band of the amide. All the observed bands revealed that the surface of the Fe_3O_4 NPs was successfully modified with organic moieties, in agreement with the results reported in the literature.[41]

To examine the thermal stability and the organic moiety loaded on the surface of the MNPs, thermogravimetric analysis was used. Fig. 2(a) shows the typical TGA curve of Fe_3O_4-APTMS. The initial weight loss up to 250 °C was probably due to the removal of surface hydroxyls and surface adsorbed water. The weight loss at 250–500 °C could be attributed mainly to the evaporation and subsequent decomposition of surface-bonded APTMS. The Fe_3O_4 MNPs can be transformed to Fe_2O_3 and the weight would increase when the temperature is above 500 °C. As shown in Fig. 2(b), the weight loss of Fe_3O_4-APTMS-DFX is much higher than that of Fe_3O_4-APTMS in the temperature range 250–500 °C, which confirms the loading of DFX on the Fe_3O_4-APTMS surface. The morphology of Fe_3O_4 nanoparticles before and after deferasirox loading was studied with scanning electron microscopy (SEM). As shown in Fig. 3(a) and (b), the nanoparticles had a small size and a uniform spherical shape. The energy dispersive spectrum (EDS) indicated the presence of Fe, O, C, Si, and N elements (Fig. 4). This analysis confirms that the magnetic nanoparticles were modified by organic moieties.

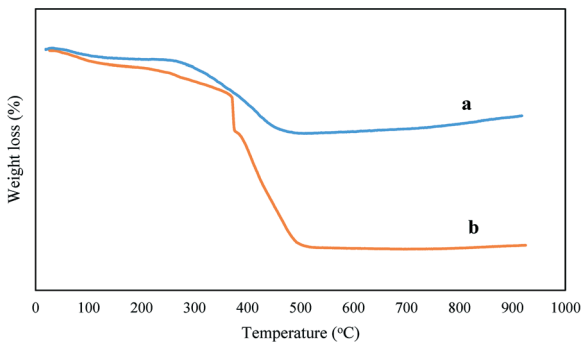

Fig. 2 TGA of (a) iron oxide nanoparticles modified with 3-(aminopropyl)trimethoxysilane (MNP-APTMS) and (b) deferasirox anchored on MNP-APTMS (MNP-APTMS-DFX).

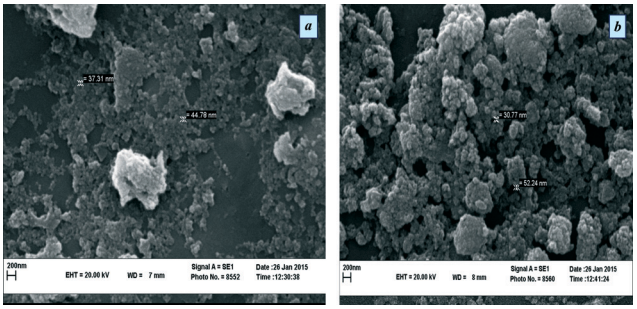

Fig. 3 SEM of: (a) Fe_3O_4 modified with 3-(aminopropyl)-trimethoxysilane (MNP-APTMS) and (b) deferasirox anchored on MNP-APTMS (MNP-APTMS-DFX).

4.1.1. The magnetization properties of magnetic nanoparticles loaded with deferasirox. The magnetic properties of the prepared MNPs were studied by vibrating sample magnetometry (VSM). The magnetic hysteresis loops of Fe_3O_4 and MNP-APTMS-DFX are shown in Fig. 5. The saturation magnetization (M_s) values at room temperature were 64.9 emu g^{-1} and 35.1 emu g^{-1}, respectively. The M_s value of MNP-APTMS-DFX was much lower than that of the Fe_3O_4 MNPs due to the silica coating and DFX loading, which provide less magnetic moment per unit mass than that of ferromagnetic core regions, which would lead to a decrease in the M_s. As shown in Fig. 5c, a dark homogeneous dispersion was observed in the absence of an external magnetic field, while in the presence of an external magnetic field, the black nanoparticles were attracted to the wall of the capped tube and the solution became transparent.

4.1.2. Dynamic light scattering and zeta-potential measurements. The hydrodynamic diameter and zeta potential of the compounds in all the steps were determined using dynamic light scattering (DLS) on a Malvern Nano ZS instrument (Malvern Instruments, UK). The results are presented as mean ± SD for three independent measurements (Table 1). The particle size of MNPs-APTMS was 44 nm, which was reduced after loading of DFX. Due to the presence of the amino group, MNP-APTMS conjugates had a positive zeta potential

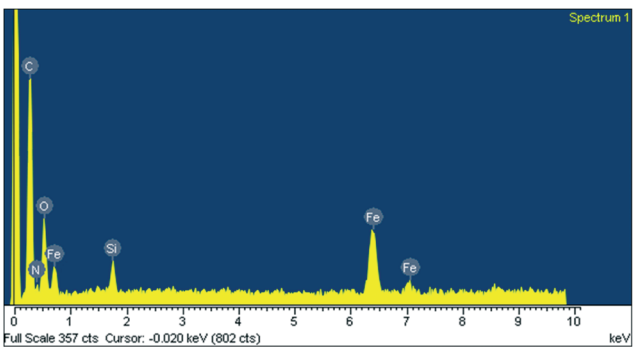

Fig. 4 The EDS spectrum of deferasirox anchored on MNP-APTMS (MNP-APTMS-DFX).

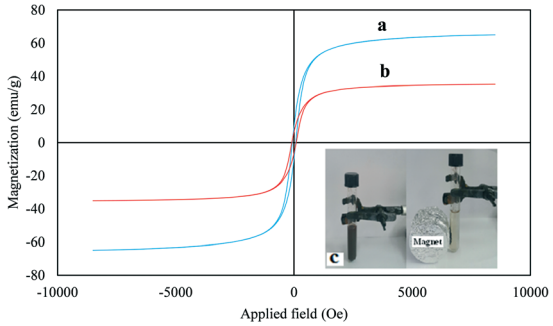

Fig. 5 Magnetization curve of the (a) bare Fe_3O_4, (b) MNP-APTMS-DFX, (c) photograph of the separation of magnetic nanoparticles under an external magnetic field.

in the range 15.1–18 mV, which decreased as the degree of loading increased. However, sufficient positive charge existed on all MNP-APTMS-DFX, which is necessary for the interaction of MNP-APTMS-DFX with negatively charged cell membranes. The particle size of all the MNP-APTMS-DFX was found to be in the range 27–38 nm by DLS analysis (Table 1), indicating a narrow size distribution.

A strong rationale for continued research into the development of new compounds with this structure improved its therapeutic application. Therefore, the newly synthesized compound was screened for its *in vitro* growth inhibitory activities against five human and animal cultured cell lines, namely human breast cancer cells (MCF-7), human cervical epithelial carcinoma (HeLa), human colon cancer cell line (HT-29), human leukemia cell line (K-562), mouse neuroblastoma cell line (Neuro-2a), and mouse fibroblast L-929 cell line, as well as normal cells, by the MTT assay method. In this study, cisplatin and MNPs were used as positive and negative controls, respectively. *In vitro* cytotoxicity of the compounds was assessed by MTT bioassay in different cancer cells after 72 h of drug exposure. We also investigated the cytotoxicity of the compounds at different incubation times, 24 and 48 h. Our results showed that our compounds do not have any cytotoxic effects on cell lines at these incubation times (24 and 48 h). The results are shown as IC_{50} values after 72 h continuous exposure (Table 2). The effect of the synthesized compound on the mouse fibroblast cell line (L-929) was evaluated as control, simultaneously. Our results confirmed that the synthesized compound has no cytotoxic effects on L-929.

Table 1 Hydrodynamic diameter and zeta potential of MNP, MNP-APTMS and MNP-APTMS-DFX

Compound	MNP	MNP-APTMS	MNP-APTMS-DFX
Dynamic light scattering DLS (nm)	70	44	35
Zeta potential (mV)	(−) 6.9 ± 1.35	(+) 16.8 ± 2.65	(+) 1.9 ± 0.43

The experiments were done in triplicate. Data were expressed as the mean of the triplicate.

5. Discussion

Magnetite nanoparticles (MNPs) have been widely used in biomedical fields due to low toxicity and good compatibility.[3,9,42,43] These are one of the FDA-approved materials used *in vivo* and have been utilized in the magnetic separation of biological entities, hyperthermia treatment, magnetic resonance imaging (MRI), and drug delivery.[9] MNPs with high magnetization values and ultrafine particle sizes can be manipulated by an external magnetic field (MF), by which human tissues can be penetrated, indicating that employing these nanoparticles for targetable drug delivery is possible.[4,44] To develop a more suitable drug delivery system composed of magnetite nanoparticles, some work needs to be done to diminish particle agglomeration, reduce cytotoxicity, and improve compatibility.[45–48] Many candidates have been considered for functionalization of MNPs to achieve these goals, including polymers, biomolecules, surfactants, and organic and inorganic materials. In this study, the potential of iron oxide nanoparticles loaded with deferasirox as effective anticancer compounds *in vitro* has been investigated. Because of interesting pharmacological activities of deferasirox, especially as anti-tumor agent,[29] treatment of toxic metals overload,[27,28] and treatment of iron overload in certain types of anaemia (β-thalassemia), ability of this drug were considered in this study.

The present study has reported the synthesis of iron oxide-based deferasirox (DFX)-loaded nanoparticles (Fe_3O_4@DFX). After characterization of magnetic nanoparticles (MNPs) by various methods, Fe_3O_4@DFX was screened for antitumor activity against MCF-7, HeLa, HT-29, K-562, Neuro-2a, and L-929 cell lines, and cisplatin was used as a comparative standard in an MTT assay. The results of the MTT assay were shown as IC_{50} values. In comparison with the IC_{50} of cisplatin, compounds with IC_{50} values less than 30 μM were considered to be strongly cytotoxic; compounds with IC_{50} values in the range 30–50 μM were considered to be moderately cytotoxic; compounds with IC_{50} values in the range of 50–100 μM were considered to be weakly cytotoxic; and compounds with IC_{50} values over 100 μM were considered to be inactive.[49]

The IC_{50} values of MNP-APTMS-DFX and cisplatin as a comparative standard were measured in all cell lines. Such measurements were done after 72 h of incubation using concentrations of several compounds in the range 20 nM to 200 μM. The selection of this concentration range was based on our investigations in previous studies. According to our knowledge, up to now only one study has investigated the anti-proliferative effects of deferasirox.[34] Higher concentrations over 200 μM are in a flat concentration range in the IC_{50} curve and can be placed in a drug-resistance range. As shown in our results, 200 μM is a non-toxic concentration to normal cells.

The IC_{50} values obtained for MNP-APTMS-DFX were between 8.50 and 89.1 μM (the cases up to 100 μM have been ignored), while those found for the cisplatin as positive

Table 2 Cytotoxic activity of MNP, MNP-APTMS and MNP-APTMS-DFX tested against MCF-7, HeLa, HT-29, K-562, Neuro-2a cancer cell lines and L-929 after 72 h continuous exposure

$IC_{50} \pm SD^a$ (μM)						
Compound	MCF-7	HeLa	HT-29	K-562	Neuro-2a	L-929
MNP	94.3 ± 7.9	155.9 ± 10.9	133.9 ± 11.8	105.1 ± 9.8	183.2 ± 11.7	241.3 ± 17.5
MNP-APTMS	87.6 ± 8.8	100.4 ± 11.5	67.0 ± 7.8	81.5 ± 7.3	106.7 ± 9.5	126.5 ± 10.7
MNP-APTMS-DFX	16.9 ± 3.53	36.1 ± 4.75	16.9 ± 2.93	8.50 ± 2.24	89.1 ± 9.53	141.3 ± 12.5
DFX	53.9 ± 6.1	35.5 ± 3.9	18.5 ± 3.62	87.9 ± 7.5	100.7 ± 9.4	102.3 ± 9.5
Cisplatin	5.94 ± 1.47	0.45 ± 0.13	19.3 ± 3.46	24.7 ± 4.71	103 ± 9.8	0.7 ± 0.2

[a] The concentration of the complex required to inhibit cell growth by 50%. The experiments were done in triplicate. Data were expressed as the mean of the triplicate. $IC_{50} > 100$ μM is considered to be inactive.

control ranged between 0.45 and 100 μM (Table 2). However, the cytotoxic activity was approximately similar for all compounds tested and was threefold more than cisplatin against the two examined cancer cell lines (HT-29 and K-562).

The IC_{50} values were obtained using deferasirox concentrations in the nanoparticles, as described by Buchman *et al.*[50] In this method, the total nitrogen in each stage was obtained by elemental analysis. We used the ninhydrin quantitative test for determination of primary amines before and after drug (deferasirox)-loading on silica nanoparticles.

Furthermore, the cytotoxic properties of Fe_3O_4-APTMS-DFX were compared to those of free deferasirox and the non-functionalized nanoparticles, and the IC_{50} values of MNP and MNP-APTMS were screened against these cancer cell lines. Our results confirmed that MNP and MNP-APTMS were either inactive against MCF-7, HeLa, HT-29, K-562, Neuro-2a, and L-929 cell lines, or exhibited very poor activity against these cancer cell lines.

In addition to cisplatin, the IC_{50} values of DFX were determined for a better comparison with the MNP-APTMS-DFX conjugate. The results presented in Table 1 confirmed that in all cell lines, magnetic nanoparticles functionalized with DFX have higher cytotoxicity compared to deferasirox. It is notable that the cytotoxicity of DFX is the same as both cisplatin and MNP-APTMS-DFX against HT-29 as a normal cell line. Based on the results of *in vitro* cytotoxicity studies of MNP-APTMS-DFX, the mechanism of its cytotoxicity was evaluated using apoptosis assay by a flow cytometry technique. The results are shown in Table 3 and Fig. 6. The four areas in the diagrams stand for necrotic cells (Q1, left square on the top), late apoptotic or necrotic cells (Q2, right square on the top), live cells (Q3, left square at the bottom), and apoptotic cells (Q4, right square at the bottom). As can be seen in Table 3 and Fig. 6, MNP-APTMS-DFX showed a high population of apoptotic cells (69.3%), nearly 1.2 fold higher than for cisplatin (58.1%) at the same concentration. Also, flow cytometry results showed that the population of apoptotic cells in DFX is more than in cisplatin but is less than in MNP-APTMS-DFX.

Nanoparticles loaded with anticancer drug were found to show a higher apoptosis-inducing effect in cancer cell lines than free drugs *in vitro*. These results are in agreement with previous reports.[51] The results of the current study demonstrated that MNP-APTMS-DFX could induce apoptosis in K-562 cancer cells. But to confirm the pro-apoptotic activity of the conjugate, further investigation is needed to better understand the precise mechanism of action of this compound, and basic animal studies are needed before it can be recommended for human administration.

The population of apoptotic cells in DFX is more than in cisplatin but is less than in MNP-APTMS-DFX.

Nanoparticles loaded with anticancer drug were found to show a higher apoptosis-inducing effect in cancer cell lines than free drugs *in vitro*. These results are in agreement with previous reports.[51] The results of the current study demonstrated that MNP-APTMS-DFX could induce apoptosis in K-562 cancer cells. But to confirm the pro-apoptotic activity of the conjugate, further investigation is needed to better understand the precise mechanism of action of this compound and basic animal studies are needed before it can be recommended for human administration.

The induction of cell death by the MNP-APTMS-DFX conjugate was confirmed to be apoptosis using the TUNEL of exposed 3′-OH termini of DNA with dUTP-FITC. As shown in the confocal laser scanning microscopy images in Fig. 7, (MNP-APTMS-DFX) treated K-562 leukemia cancer cells, examined for dUTP-FITC incorporation (green fluorescence)

Table 3 Percentages of the cell death pathways observed by the flow cytometry assay

Treatment	% vital cells	% apoptotic cells	% late apoptotic/necrotic cells	% necrotic cells
Control	77.5	16.8	4.6	1.1
DFX	35.4	32.3	28.0	4.5
MNP-APTMS-DFX	24.2	37.6	31.7	6.5
Cisplatin	34.1	30.8	27.3	7.8

These compounds were incubated for 24 h at a concentration of 5 μM, and the experiments were done in triplicate.

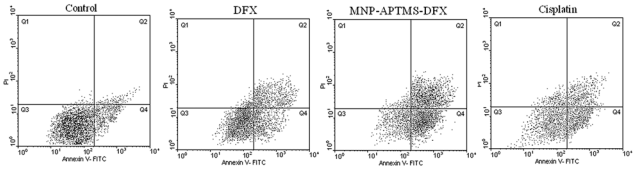

Fig. 6 Flow cytometric results after the exposure of K-562 cancer cells. Four areas in the diagrams represent four different cell states: necrotic cells (Q1), late apoptotic or necrotic cells (Q2), living cells (Q3) and apoptotic cells (Q4).

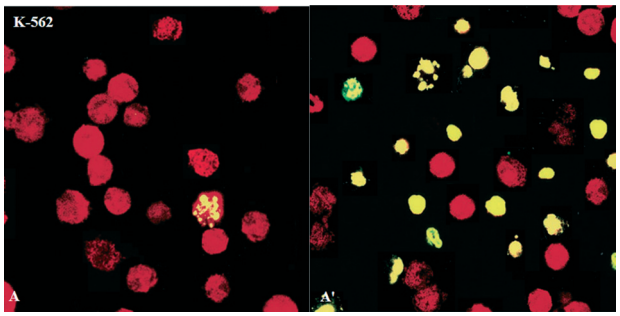

Fig. 7 MNP-APTMS-DFX induction of apoptosis in human leukemia cancer cells (K-562). Leukemia cancer cells (K-562) (A, A′) cells after being incubated with 10 μM of MNP-APTMS-DFX for 24 h, fixed, permeabilized and visualized for DNA degradation in a TUNEL assay using dUTP-labeling. Red fluorescence, nuclei stained with propidium iodide. Green or yellow (*i.e.*, superimposed red and green) fluorescence, apoptotic nuclei containing fragmented DNA. When compared with control and treated with 0.3% DMSO (A), several cells incubated with MNP-APTMS-DFX (A′) exhibited apoptotic nuclei.

and propidium iodide counterstaining (red fluorescence), exhibited many apoptotic yellow nuclei (superimposed green and red fluorescence) at 24 h after treatment.

6. Conclusion

In this work, the synthesis, full characterization and anticancer activity of a novel series of deferasirox-loaded iron oxide nanoparticles are reported. Because of the interesting cytotoxic activity of deferasirox, we used it in this investigation. Furthermore, magnetic nanoparticles decorated with different ligands are potentially useful for cancer imaging and treatment; we developed a nanoparticulate system to include these characteristics and tested it *in vitro* for its potential cytotoxic activity. Our results confirmed the excellent cytotoxic activities of MNP-APTMS-DFX against the human leukemia cell line (K-562), compared to other cell lines. Also, our results confirmed that the investigated compound produced a higher population of apoptotic cells than cisplatin. The pharmacological results also suggest that the studied compound, MNP-APTMS-DFX, is a potent anticancer agent. In particular, it has been proven that the cytotoxicity of magnetic nanoparticles functionalized with DFX is higher than the drug (DFX), MNP-APTMS, and MNP.

Acknowledgements

The authors gratefully acknowledge the partial support of this study (Grant No: 41256) by Ferdowsi University of Mashhad Research Council. We are grateful for help provided by Buali Research Institute, School of Pharmacy, Mashhad University of Medical Sciences, Mashhad, Iran.

Notes and references

1 M. Faraji, Y. Yamini and M. Rezaee, *J. Iran. Chem. Soc.*, 2010, **7**, 1–37.
2 J. Dobson, *Drug Dev. Res.*, 2006, **67**, 55–60.
3 A. K. Gupta and M. Gupta, *Biomaterials*, 2005, **26**, 3995–4021.
4 T. Neuberger, B. Schopf, H. Hofmann, M. Hofmann and B. Rechenberg, *J. Magn. Magn. Mater.*, 2005, **293**, 483–496.
5 E. Duguet, S. Vasseur, S. Mornet and J. M. Devoisselle, *Nanomedicine*, 2006, **1**, 157–168.
6 M. Mitsumori, M. Hiraoka, T. Shibata, Y. Okuno, S. Masunaga, M. Koishi, K. Okajima, Y. Nagata, Y. Nishimura, M. Abe, K. Ohura, M. Hasegawa, H. Nagae and Y. Ebisawa, *Int. J. Hyperthermia*, 1994, **10**, 785–793.
7 D. Dorniani, M. Z. Bin Hussein, A. U. Kura, S. Fakurazi, A. Halim Shaari and Z. Ahmad, *Int. J. Nanomed.*, 2012, **7**, 5745–5756.
8 S. Prijic and G. Sersa, *Radiol. Oncol.*, 2011, **45**, 1–16.
9 Q. A. Pankhurst, J. Connolly, S. Jones and J. Dobson, *J. Phys. D: Appl. Phys.*, 2003, **36**, R167–R181.
10 A. S. Arbab, L. A. Bashaw, B. R. Miller, E. K. Jordan, B. K. Lewis, H. Kalish and J. A. Frank, *Radiology*, 2003, **229**, 838–846.
11 A. Jordan, R. Scholz, P. Wust and R. Felix, *J. Magn. Magn. Mater.*, 1999, **201**, 413–419.
12 A. Jordan, R. Scholz, P. Wust, H. Schirra, T. Schiestel and R. Felix, *J. Magn. Magn. Mater.*, 1999, **194**, 185–196.
13 S. Gustafsson, A. Fornara, K. Petersson, C. Johansson, M. Muhammed and E. Olsson, *Cryst. Growth Des.*, 2010, **10**, 2278–2284.
14 A. H. Lu, E. L. Salabas and F. SchÜth, *Angew. Chem., Int. Ed.*, 2007, **46**, 1222–1244.
15 S. Libertino, F. Giannazzo, V. Aiello, A. Scandurra, F. Sinatra, M. Renis and M. Fichera, *Langmuir*, 2008, **24**, 1965–1972.
16 E. Mälkilä, L. M. Bimbo, M. Kaasalainen, B. Herranz, A. J. Airaksinen, M. Heinonen, E. Kukk, J. Hirvonen, H. A. Santos and J. Salonen, *Langmuir*, 2012, **28**, 14045–14054.
17 R. Chen, Y. Jiang, W. Xing and W. Jin, *Ind. Eng. Chem. Res.*, 2011, **50**, 4405–4411.
18 M. Mahmoudi, M. A. Sahraian, M. A. Shokrgozar and S. Laurent, *ACS Chem. Neurosci.*, 2011, **2**, 118–140.
19 T. N. Van, Y. K. Lee, J. Lee and Y. Park, *Langmuir*, 2013, **29**, 3054–3060.
20 A. P. Taylor, R. I. Webb, J. C. Barry, H. Hosmer, R. J. Gould and B. J. Wood, *J. Microsc.*, 2000, **199**, 56–67.
21 A. Rezania, R. Johnson, A. R. Lefkow and K. E. Healy, *Langmuir*, 1999, **15**, 6931–6939.

22 Z. Liu, Z. Li, H. Zhou, G. Wei, Y. Song and L. J. Wang, *J. Microsc.*, 2005, **218**, 233–239.
23 Y. H. Deng, C. C. Wang, J. H. Hu, W. L. Yangand and S. K. Fu, *Colloids Surf., A*, 2005, **262**, 87–93.
24 G. F. Paciotti, *Drug Delivery*, 2004, **11**, 169–183.
25 U. Heinz, K. Hegetschweiler, P. Acklin, B. Faller and R. Lattmann, *Angew. Chem., Int. Ed.*, 1999, **38**, 2568–2571.
26 L. P. H. Yang, S. J. Keam and G. M. Keating, *Drugs*, 2007, **67**, 2211–2230.
27 A. Sh. Saljooghi and S. J. Fatemi, *BioMetals*, 2010, **23**, 707–712.
28 A. Sh. Saljooghi and S. J. Fatemi, *J. Appl. Toxicol.*, 2011, **31**, 139–143.
29 M. Whitnall, J. Howard, P. Ponka and D. R. Richardson, *Proc. Natl. Acad. Sci. U. S. A.*, 2006, **103**, 14901–14906.
30 R. Lattmann and P. Acklin, *PCT Int. Appl.*, WO9749395A1 Novartis Pharma AG, 1997; *Chem. Abstr.*, 1998, **128**, 114953e.
31 Y. I. Ryabukhin, L. N. Faleeva and V. G. Korobkova, *Chem. Heterocycl. Compd.*, 1983, **19**, 332–336.
32 R. Massart, E. Dubois, V. Cabuil and E. Hasmonay, *J. Magn. Magn. Mater.*, 1995, **149**, 1–5.
33 B. Z. Tang, Y. Geng, J. W. Y. Lam, B. Li, X. Jing, X. Wang, F. Wang, A. B. Pakhomov and X. X. Zhang, *Chem. Mater.*, 1999, **11**, 1581–1589.
34 G. Y. L. Lui, P. Obeidy, S. J. Ford, C. Tselepis, D. M. Sharp, P. J. Jansson, D. S. Kalinowski, Z. Kovacevic, D. B. Lovejoy and D. R. Richardson, *Mol. Pharmacol.*, 2013, **83**, 179–190.
35 Z. Salmasi, W. T. Shier, M. Hashemi, E. Mahdipour, H. Parhiz, K. Abnous and M. Ramezani, *Eur. J. Pharm. Biopharm.*, 2015, **96**, 76–88.
36 F. Silva, F. Marques, I. C. Santos, A. Paulo, A. Sebastião Rodrigues, J. Rueff and I. Santos, *J. Inorg. Biochem.*, 2010, **104**, 523–532.
37 R. K. Narla, Y. Dong, O. J. D'Cruz, C. Navara and F. M. Uckun, *Clin. Cancer Res.*, 2000, **6**, 1546–1556.
38 D. M. Zhu, R. K. Narla, W. H. Fang, N. C. Chia and F. M. Uckun, Calphostin, *Clin. Cancer Res.*, 1998, **4**, 2967–2976.
39 S. Mohapatra, N. Pramanik, S. Mukherjee, S. K. Ghosh and P. J. Pramanik, *Mater. Sci.*, 2007, **42**, 7566–7574.
40 M. Shen, H. Cai, X. Wang, X. Cao, K. Li, S. H. Wang, R. Guo, L. Zheng, G. Zhang and X. Shi, *Nanotechnology*, 2012, **23**, 105601–105610.
41 M. Esmaeilpour, J. Javidi, F. Nowroozi and M. Mokhtari, *J. Mol. Catal. A: Chem.*, 2014, **393**, 18–29.
42 Q. Pankhurst, N. Thanh, S. Jones and J. Dobson, *J. Phys. D: Appl. Phys.*, 2009, **42**, 224001–224007.
43 P. Tartaj, M. P. Morales, S. Veintemillas-Verdaguer, T. Gonzàlez-Carreno and C. J. Serna, *J. Phys. D: Appl. Phys.*, 2003, **36**, R182–R197.
44 V. I. Shubayev, T. R. Pisanic and S. Jin, *Adv. Drug Delivery Rev.*, 2009, **61**, 467–477.
45 J. L. Zhang, R. S. Srivastava and R. D. K. Misra, *Langmuir*, 2007, **23**, 6342–6351.
46 T. J. Brunner, P. Wick, P. Manser, P. Spohn, N. Robert, L. K. Limbach, A. Bruinink and W. Stark, *J. Environ. Sci. Technol.*, 2006, **40**, 4374–4381.
47 U. O. Häfeli and G. J. Pauer, *J. Magn. Magn. Mater.*, 1999, **194**, 76–82.
48 J. S. Kim, T. J. Yoon, K. N. Yu, B. G. Kim, S. J. Park, H. W. Kim, K. H. Lee, S. B. Park, J. K. Lee and M. H. Cho, *Toxicol. Sci.*, 2006, **89**, 338–347.
49 H. Liu, F. Zhao, R. Yang, M. Wang, M. Zheng, Y. Zhao, X. Zhang, F. Qiu and H. Wang, *Phytochemistry*, 2009, **70**, 773–778.
50 Y. K. Buchman, E. Lellouche, S. Zigdon, M. Bechor, S. Michaeli and J. P. Lellouche, *Bioconjugate Chem.*, 2013, **24**, 2076–2087.
51 A. Javid, S. Ahmadian, A. A. Saboury, S. M. Kalantar and S. Rezaei-Zarchi, *RSC Adv.*, 2014, **4**, 13719–13728.